Folded and unfolded conformations of the omega-3 polyunsaturated fatty acid family: CH3CH2[CH=CHCH2](B)[CH2](M)COOH. First principles study

ARTICLE *in* THE JOURNAL OF PHYSICAL CHEMISTRY A · JUNE 2006

Impact Factor: 2.69 · DOI: 10.1021/jp058215o · Source: PubMed

ELSEVIER

Journal of Molecular Structure: THEOCHEM 725 (2005) 111–125

THEO CHEM

www.elsevier.com/locate/theochem

Selenocysteine derivatives I. Sidechain conformational potential energy surface of *N*-acetyl-L-selenocysteine-*N*-methylamide (MeCO-L-Sec-NH-Me) in its β_L backbone conformation

Imre L. Hegedűs[a], Michelle A. Sahai[a,b,c], Máté Labádi[a], Milán Szőri[a], Gábor Paragi[b,d], Bela Viskolcz[a,*], Andrea Bottoni[e]

[a]*Department of Chemistry and Chemical Informatics, JGyTFK, University of Szeged, P.O. Box 396, 6701 Szeged, Hungary*
[b]*Department of Medical Chemistry, University of Szeged, Dóm tér 8, 6720 Szeged, Hungary*
[c]*Department of Medical Biophysics, University of Toronto, Ontario Cancer Institute, Princess Margaret Hospital, 610 University Avenue, Rm. 7-611, Toronto, Ont., Canada M5G 2M9*
[d]*Protein Chemistry Research Group, Hungarian Academy of Sciences, University of Szeged, Dóm tér 8, 6720 Szeged, Hungary*
[e]*Dipartimento di Chimica 'G. Ciamician', Università degli Studi di Bologna, via Selmi 2, 40126 Bologna, Italy*

Received 1 November 2004; accepted 31 January 2005

Abstract

Selenocysteine is expected to have $9^2=81$ conformations [in the backbone: $\psi(g^+,a,g^-)\times\varphi(g^+,a,g^-)$; $3^2=9$ and in the sidechain: $\chi^1(g^+,a,g^-)\times\chi^2(g^+,a,g^-)$; $3^2=9$]. All torsional modes of the sidechain (χ^1: rotation about the C^α–C^β and χ^2: rotation about the C^β–Se bonds) were investigated in the relaxed β_L backbone [(ψ,φ), (a,a)] conformation. The relaxed potential energy surface (PES) obtained at the RHF/3-21G level of theory contained seven out of nine possible minima of the sidechain. All minima were re-optimized at the RHF/6-31G(d) and the B3LYP/6-31G(d) levels of theory. Two of the minima (g^+a) and (g^-g^+) located at RHF/3-21G level of theory were annihilated when optimized at higher levels of theory. The frequency calculations for the found minima were used to construct the thermodynamic functions. The relative energies of the $-CH_2-SeH$ sidechain conformations have been compared with the relative energies of the analogous $-CH_2-SH$ and $-CH_2-OH$ sidechain conformers. Oxidative dimerization energies were also estimated.

Keywords: Selenocysteine (Sec); Oxidative stress; Antioxidants; Peptide folding; Quantum chemistry; Molecular conformations; Potential energy surface (PES); Se–S and Se–Se linkage

1. Introduction

1.1. Oxidative stress

One of the major current theories of aging and the origin of numerous age-related degenerative diseases is associated with a variety of free radical reactions within the human body [1–3]. All oxygen-consuming organisms, including animals and plants, are subject to the same type of attacks [4]. The effects of these reactions are collectively referred to as oxidative stress [2].

The free radicals are mainly the result of the by-products of redox reactions associated with metabolism. The free radicals include the super-oxide anion (O_2^-), the hydroperoxyl radical (HOO), and the hydroxyl radical (HO) [5]. These are collectively referred to as 'reactive oxygen species' (ROS) [3]. The production of these ROS is illustrated in Fig. 1. They are all very reactive in the body and are therefore short-lived. Normally, there are natural mechanisms defending against the free radicals within the body. However, if for some reason these defense mechanisms, which can be either enzymatic [6] or non-enzymatic [7], become weakened, then the free radicals can react with cellular structures like DNA as well as proteins or destroy membranes through lipid peroxidation [8–10].

It has been unequivocally demonstrated that almost all types of stress in plants will change its internal redox

* Corresponding author.
E-mail address: viskolcz@jgytf.u-szeged.hu (B. Viskolcz).

0166-1280/$ - see front matter © 2005 Elsevier B.V. All rights reserved.
doi:10.1016/j.theochem.2005.01.045

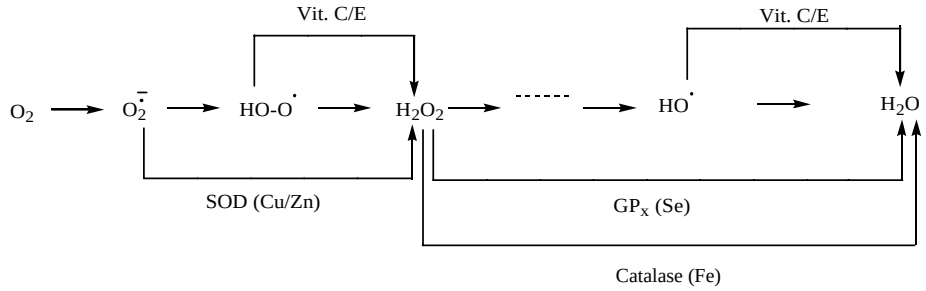

Fig. 1. Sequential reduction of H_2O_2 to H_2O. Note that Glutathione peroxidase [GP_x(Se)] is catalyzing the direct conversion of one molecule of H_2O_2 to two molecules of H_2O.

condition; in other words, stress will shift its metabolism towards oxidation. [11]. Clearly, the situation may be analogous in animals and human beings. Such 'induced' oxidative stress is in addition to the 'normal' oxidative stress that result in up to 5% of inhaled oxygen escaping the normal reductive route in the form of ROS [2,5].

It is worth mentioning examples of enzymatic and non-enzymatic mechanisms of defense starting with the enzyme glutathione peroxidase (GP_x) [6,12], which will lead to the focus of this paper. As illustrated in Fig. 2 [13], GP_x is responsible for one of the enzymatic processes that combat oxidative stress. The overall involvement of glutathione [14] as an antioxidant is shown in Fig. 3.

Selenocysteine (Sec) [7] plays an important role at the active site of the enzyme gluthatione peroxidase. It is an enzyme that converts H_2O_2 to two moles of H_2O, and has already been studied [12,15–17]. In connection with the non-enzymatic removal of the damaging ROS, the structure and isomerization of lycopene [18–20] has been investigated. The free radical scavenging mechanism of Vitamin E [21–25] and Vitamin C [26,27] have also been investigated, while some ab initio computations on flavones [28,29] have also been published.

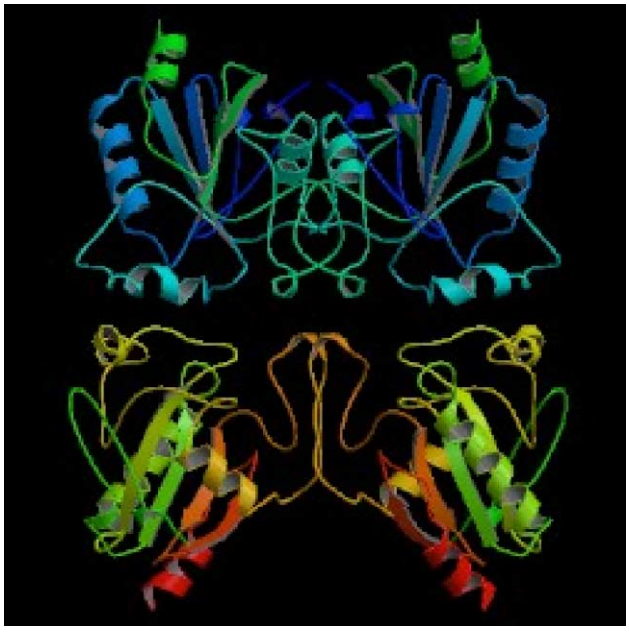

Fig. 2. Ribbon structures of glutathione peroxidase fighting against oxidative stress.

1.2. Structural characteristics

As previously mentioned, GP_x represents an important example of an antioxidant. The selenium (Se) included in the Sec residue of the enzyme's catalytic site is particularly important for its activity. Sec by itself would therefore be an important focal point for conformational analysis as it plays a significant role in the GP_x catalytic cycle illustrated in Fig. 3.

However, by comparing the structural characteristics, that is, the conformational similarities and differences of Sec and other amino acids involved in enzymatic activity (selenocysteine, cysteine and serine: $–CH_2SeH$, $–CH_2SH$ and $–CH_2OH$ groups), one could assign Sec to a particularly important role in Fig. 3. Elementary knowledge of the periodic table would verify that the Se atom is larger than both the S and the O atoms and has longer bond lengths. As a result, the Se atom has greater polarizability, and is therefore a better nucleophile. For this reason, one may expect interactions within Sec to occur between the Se atom from the sidechain and the oxygen or nitrogen atoms of the backbone amide groups [17,30].

These particular characteristics will be analyzed and presented in this work in terms of geometric preferences,

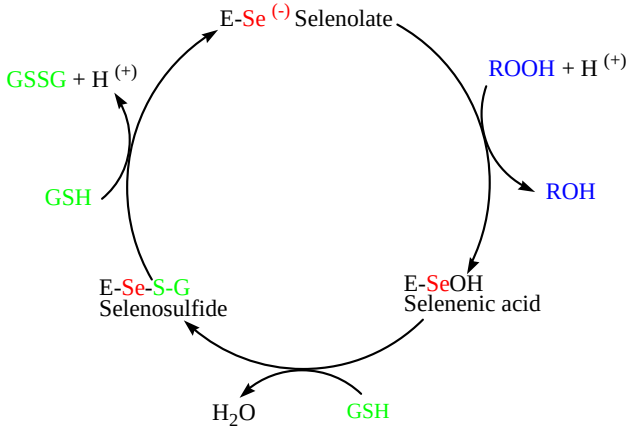

Fig. 3. Biochemical pathway of glutathione peroxidase [$E–Se^-$ or GP_x(Se)].

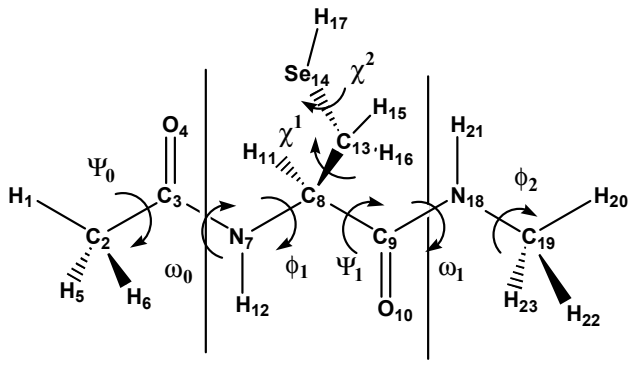

Fig. 4. MeCO-β_L-Sec-NH-Me this β_L backbone conformation. Torsion angles ω_0, ω_1, φ_1, ψ_1, χ^1 and χ^2 are shown.

as well as calculations of the thermodynamic functions for energetically stable minima.

2. Methods

2.1. Conformational analysis

A modular numbering system was adopted such that the molecule was divided into three sections: the amino acid residue and the *N*- and *C*-protective groups. Each section was numbered separately. This modular system allows the protective groups to be removed and replaced by other amino acids, thus facilitating the use of our results in future studies on oligopeptides [31,32]. The numbering system and definitions of dihedral angles of interest are shown in Fig. 4. In accordance with the IUPAC-IUB [33] recommendations, all dihedral angles were described within -180.0; and 180.0° for the backbone, i.e. BB (ϕ,ψ) and sidechain i.e. SC (χ^1,χ^2) conformations as well as the isomerism of the peptide bond (ω_0,ω_1):

$$-180 \le \phi \le 180^\circ \quad (1a)$$

$$-180 \le \psi \le 180^\circ \quad (1b)$$

$$-180 \le \chi^1 \le 180^\circ \quad (1c)$$

$$-180 \le \chi^2 \le 180^\circ \quad (1d)$$

$$-180 \le \omega_0 \le 180^\circ \quad (1e)$$

$$-180 \le \omega_1 \le 180^\circ \quad (1f)$$

2.2. Molecular computations

The computational study of the total surface requires $12 \times 12 = 144$ SCF points if the grid search is executed at 30° increments at the RHF/3-21G level of theory. Geometry optimizations were performed with GAUSSIAN 03 [34] at the RHF/6-31G(d) and B3LYP/6-31G(d) levels of theory for those minima that were shown to exist on the PES generated at the RHF/3-21G level of theory. Use of the 6-31G(d) basis set was justified, as it is a well-established fact that the role of d-type basis functions is essential for the description of hyper-valent compounds of second-row elements such as Sec [35].

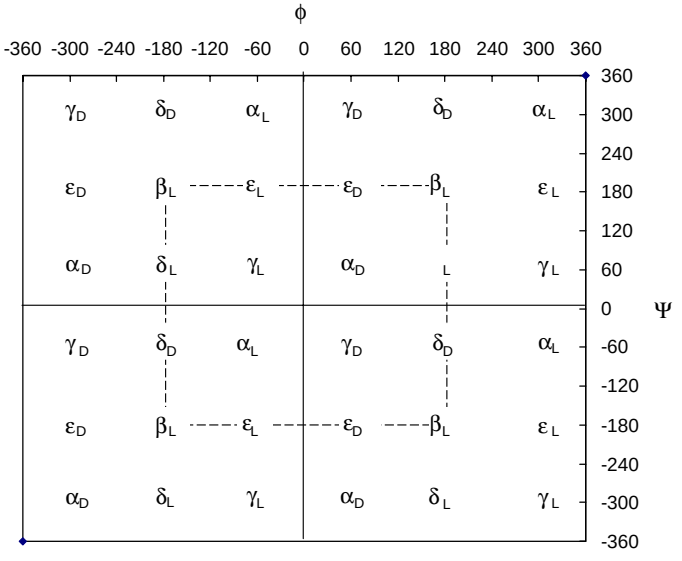

Fig. 5. Topological representation of the Ramachandran map an *N*- and *C*-protected amino acid CH_3–CO–NH–CHR–CO–$NHCH_3$ showing two full cycle of rotation $-360 \le \varphi \le +360°$; $-360 \le \psi \le 360°$. The central box, denoted the by broken line represents the cut suggested by the IUPAC conversation ($-180 \le \varphi \le +180°$; $-180 \le \psi \le 180°$). The four quadrants denoted by solid lines are the conventional cuts (e.g. $0 \le \varphi \le +360°$; $0 \le \psi \le 360°$). Most *L*-peptide residues exhibit nine unique conformations labeled as α_L, β_L, γ_L, δ_L, ε_L, α_D, β_D, γ_D, δ_D, and ε_D.

3. Results and discussion

3.1. Conformational geometries

On the basis of multidimensional conformational analysis (MDCA) [36] since *N*- and *C*-protected Sec has four rotors (ψ,ϕ,χ^1,χ^2), one may expect three minima (g^+,a,g^-) along each of the variables, leading to $3^4=81$ conformers. Of these, there are $3^2=9$ backbone (BB) conformers; for each of the backbone conformers there are $3^2=9$ sidechain (SC) conformers.

Fig. 5 shows the topological representation of the ideal Ramachandran map of an *N*- and *C*-protected amino acid CH_3–CO–NH–CHR–CO–$NHCH_3$ showing two full cycle of rotation: $-360\leq\phi\leq+360°$as well as $-360\leq\psi\leq+360°$. The central box, denoted the by broken line, represents the cut suggested by the IUPAC conversation ($-180\leq\phi\leq+180°$ and $-180\leq\psi\leq+180°$). The four quadrants denoted by solid lines are the conventional cuts (e.g. $0\leq\phi\leq+360°$; $0\leq\psi\leq+360°$). Most peptide containing L-amino acid residues exhibit nine unique conformations labeled as α_L, β_L, γ_L, δ_L, ε_L, α_D, β_D, γ_D, δ_D, and ε_D.

Fig. 6 depicts the sidechain potential energy surfaces, $E=E(\chi^1,\chi^2)$, for *N*-acetyl-*L*-selenocysteine-*N*-methylamide (as MeCO-L-Sec-NH-Me for short) in its β_L backbone conformation. The two dihedral angles of the sidechain are defined in Fig. 4. A landscape presentation is presented at the top of the figure while at the bottom; an energy contour diagram is seen. It should be noted that the (g^+a) and (g^+g^-) minima exist only at RHF/3-21G level of theory.

In Table 1 the dihedral angles of the backbone and the sidechain obtained for all existing conformers of MeCO-L-Sec-NH-Me obtained at the RHF/3-21G, RHF/6-31G(d) and B3LYP/6-31G(d) levels of theory are compared. The backbone structure does not vary very much, but there is a significant difference between the values of some of the types of dihedral angles. For example, ψ_0 and ω_0 in the g^-g^- conformer differ considerably with respect to all

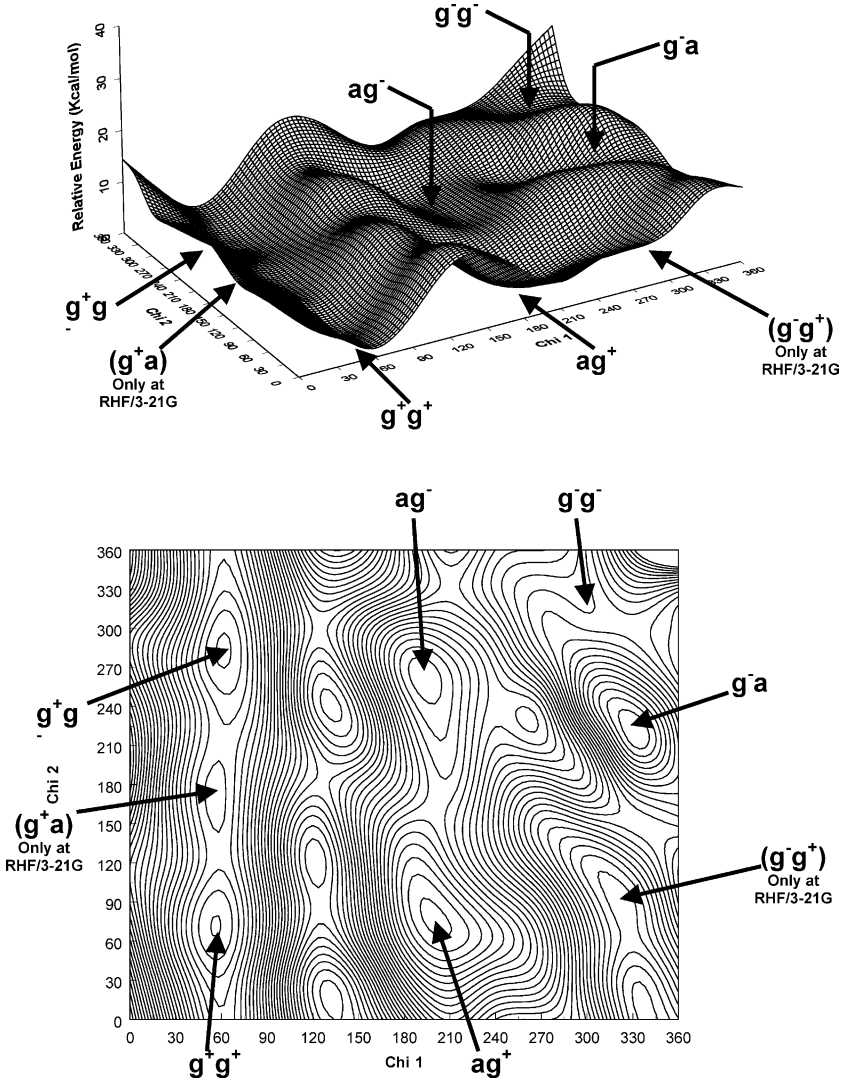

Fig. 6. $E=E(\chi^1,\chi^2)$ for MeCO-L-Sec-NH-Me in its β_L backbone conformation. Top: landscape presentation bottom: energy contour diagram.

Table 1
Selected parameters of conformers of backbone and sidechain of MeCO-L-Sec-NH-Me obtained at the B3LYP/6-31G(d) level of theory. Torsion angles (ψ,φ,χ^1,χ^2,ω_0,ω_1) are given in degrees in IUPAC-IUB convention

Calculation	Conformation			ψ_0	ω_0	φ_1	ψ_1	ω_1	φ_2	χ^1	χ^2	Energy	
Level of theory	BB	χ^1	χ^2									Hartrees	kcal mol^{-1}
RHF/3-21G	β_L	g^+	g^+	−178.15	−179.79	−168.84	171.29	178.65	−122.39	56.76	73.17	−2878.595690	0.52
		g^+	a	−177.50	179.29	−168.06	172.76	178.14	−119.79	54.27	164.37	−2878.594460	1.29
		g^+	g^-	178.13	176.53	−166.34	174.70	178.37	−120.63	61.86	−67.72	−2878.595790	0.46
		a	g^+	178.69	177.52	−168.23	169.49	178.78	173.36	−164.64	82.33	−2878.596520	0.00
		a	a	Not found—migrated to β_L [ag^-]									
		a	g^-	179.44	178.54	−166.15	160.17	178.96	−173.01	−171.64	−86.11	−2878.595500	0.64
		g^-	g^+	177.28	173.04	−122.50	157.83	176.77	−122.86	−164.42	83.04	−2878.592310	2.64
		g^-	a	−177.91	176.27	−146.50	161.82	177.30	−121.28	−68.49	−177.86	−2878.591830	2.94
		g^-	g^-	−176.38	178.01	−137.78	158.15	176.70	−121.81	−57.09	−48.00	−2878.592550	2.49
RHF/6-31G(d)	β_L	g^+	g^+	−157.94	−179.57	−159.19	172.08	−176.14	−167.66	59.32	84.16	−2890.431400	2.82
		g^+	a	Not found—migrated to β_L [g^+g^+]									
		g^+	g^-	151.05	170.90	−155.21	177.74	−178.14	−169.50	66.68	−70.51	−2890.431460	2.79
		a	g^+	−96.43	173.34	−158.65	165.98	175.87	172.51	−161.62	67.72	−2890.435900	0.00
		a	a	Not found—migrated to β_L [ag^-]									
		a	g^-	144.66	175.24	−158.10	155.24	175.14	169.23	−169.25	−94.35	−2890.434870	0.65
		g^-	g^+	Not found—migrated to β_L [ag^+]									
		g^-	a	−153.07	−179.23	−141.01	147.46	179.85	−166.79	−65.85	177.66	−2890.428300	4.77
		g^-	g^-	−158.57	−170.65	−138.74	132.92	−178.48	−166.10	−52.47	−61.90	−2890.430340	3.49
B3LYP/6-31G(d)	β_L	g^+	g^+	−107.96	175.48	−158.73	174.98	−177.25	−143.94	60.18	85.62	−2895.223480	4.37
		g^+	a	Not found—migrated to β_L [g^+g^+]									
		g^+	g^-	127.95	173.30	−160.79	−179.73	178.13	179.71	68.06	−63.75	−2895.223430	4.41
		a	g^+	127.54	172.70	−159.27	173.11	177.46	140.93	−164.42	63.27	−2895.230450	0.00
		a	a	Not found—migrated to β_L [ag^-]									
		a	g^-	125.42	174.77	−159.57	165.47	176.74	−99.09	−168.00	−100.57	−2895.229062	0.87
		g^-	g^+	Not found—migrated to β_L [ag^+]									
		g^-	a	107.84	175.91	−143.99	158.26	−179.79	−149.40	−67.37	−178.60	−2895.221100	5.87
		g^-	g^-	−151.14	−177.21	−138.84	142.45	179.10	−135.42	−51.28	−62.71	−2895.222030	5.28

the other conformers. There are only apparent differences between the angles near −180° and the angles near +180° because there is continuity in the two borders of the limiting angle values (i.e. −180° is equivalent to +180°). The two terminal ends of the backbone structure about the C(2)–C(3) and N(18)–C(19) axes corresponding to methyl rotations (ψ_0 and ϕ_2) have virtually free rotation. The conformational geometries as exemplified by the six torsional angles

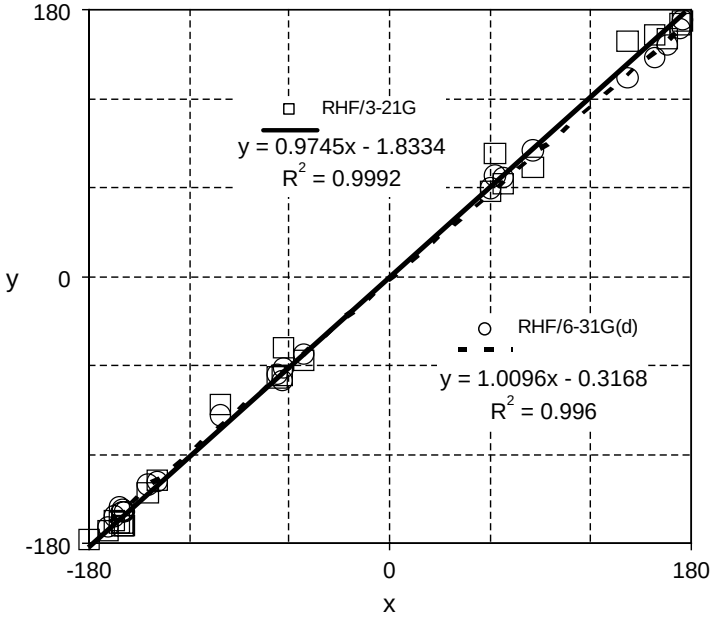

Fig. 7. Correlation of RHF computed dihedral angles (y) with DFT computed dihedral angles (x).

Table 2
Energetics and thermochemistry for various sidechain conformations of MeCO-L-Sec-NH-Me at it's β_L backbone conformation computed at the B3LYP/6-31G(d) level of theory specified by the DFT frequency calculation

Parameters		ag^-	ag^+	g^-g^-	g^-a	g^+g^+	g^+g^-
Sum of electronic and zero-point energies: E	(Hartrees)	−2895.0434	−2895.0449	−2895.0372	−2895.0363	−2895.0388	−2895.0391
Sum of electronic and thermal energies: U		−2895.0296	−2895.0311	−2895.0231	−2895.0222	−2895.0246	−2895.0249
Sum of electronic and thermal enthalpies: H		−2895.0287	−2895.0302	−2895.0221	−2895.0213	−2895.0237	−2895.0240
Sum of electronic and thermal free energies: G		−2895.0867	−2895.0881	−2895.0811	−2895.0804	−2895.0834	−2895.0835
Relative zero-point energies: ΔE	(kcal mol^{-1})	0.9281	0.0000	4.8212	5.3577	3.8266	3.6276
Relative thermal energies: ΔU		0.9281	0.0000	5.0496	5.5760	4.0619	3.8874
Relative thermal enthalpies: ΔH		0.9281	0.0000	5.0496	5.5760	4.0619	3.8874
Relative thermal free energies: ΔG		0.8904	0.0000	4.3687	4.8400	2.9298	2.8709

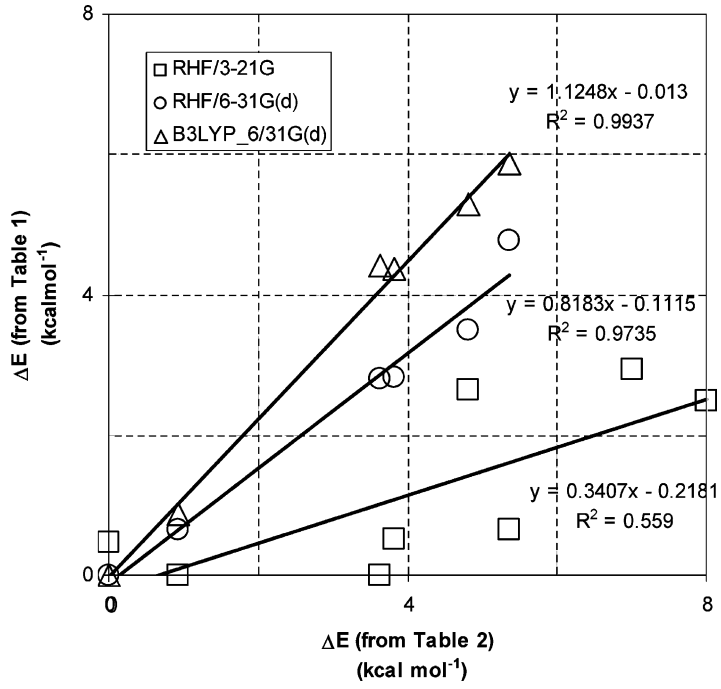

Fig. 8. Correlation of computed relative energies including zero-point vibrational energy (ZPE) correlated ΔE values computed at various levels of theory.

(ϕ, ψ, χ^1, χ^2, ω_0 and ω_1) are compared in Fig. 7. The lower level RHF results differ somewhat from the DFT values. We should observe that the global minimum is the ag^+ conformer at all levels of theory.

3.2. Conformational stabilities

Conformational stabilities measured by the relative energies cover a noticeable range, as summarized in Table 1.

Table 3
Calculation of the characteristics of conformational position vectors to be used as structural descriptors

Calculation (level of theory)	Conformation			χ^1	χ^2	$\Delta\chi^1$	$\Delta\chi^2$	$\Delta\chi^1/\Delta\chi^2$	τ	sin τ	sin$^2\tau$
	BB	χ^1	χ^2								
B3LYP/6-31G(d)	β_L	g^+	g^+	60.18	85.62	−119.82	−94.38	0.788	−0.667	−0.619	0.383
		g^+	a	Not found—migrated to β_L [g^+g^+]							
		g^+	g^-	68.06	−63.75	−111.94	116.25	−1.039	0.804	0.720	0.519
		a	g^+	−164.42	63.27	15.58	−116.73	−7.492	−1.438	−0.991	0.982
		a	a	Not found—migrated to β_L [ag^-]							
		a	g^-	−168.00	−100.57	12.00	79.43	6.619	1.421	0.989	0.978
		g^-	g^+	Not found—migrated to β_L [ag^+]							
		g^-	a	−67.37	−178.60	112.63	1.40	0.012	0.012	0.012	0.000
		g^-	g^-	−51.28	−62.71	128.72	117.29	0.911	0.739	0.674	0.454

For example, the (g^-a) conformer exhibited relative energies of 2.94, 4.77 and 5.87 kcal/mol at the RHF/3-21G, RHF/6-31G(d) and B3LYP/6-31G(d)levels of theory, respectively.

Computed thermodynamic functions are compared in Table 2. These thermodynamic functions (E, U, H, G) were obtained after the appropriate frequency calculations at the B3LYP/6-31G(d) level of theory. A comparison of the energies obtained at the various levels is shown in Fig. 8.

Some data was generated with certain manipulations of χ^1 and χ^2 (Table 3) in order to correlate stability with geometry. In the first step, χ^1 and χ^2 were shifted to a new origin at $\chi^1=\chi^2=180°$ (the fully anti arrangement). From that origin, $\Delta\chi^1$ and $\Delta\chi^2$ measured the change of the rotational angle of the position vector. The above shift was achieved by subtracting 180° if χ^1 and χ^2 were positive, or adding 180° if these dihedral angles were negative:

$$\Delta\chi^i = \chi^i - 180° \quad \text{for } \chi^i > 0 \tag{2a}$$

$$\Delta\chi^i = \chi^i + 180° \quad \text{for } \chi^i < 0 \tag{2b}$$

The tangent of the angle of rotation of a position vector, with the $\Delta\chi^1$ and $\Delta\chi^2$ as its vectorial components were defined as the ratio of $\Delta\chi^1/\Delta\chi^2$ from which the angle of rotation (τ) could be calculated:

$$\tau = \text{arctg}(\Delta\chi^1/\Delta\chi^2). \tag{3}$$

The extent of rotation of that position vector as shown in Fig. 9 may be measured by τ, or some trigonometric functions of τ such as sin or $\sin^2$

$$\sin\tau = \sin[\text{arctg}(\Delta\chi^1/\Delta\chi^2)] \tag{4}$$

$$\sin^2\tau = \sin^2[\text{arctg}(\Delta\chi^1/\Delta\chi^2)]. \tag{5}$$

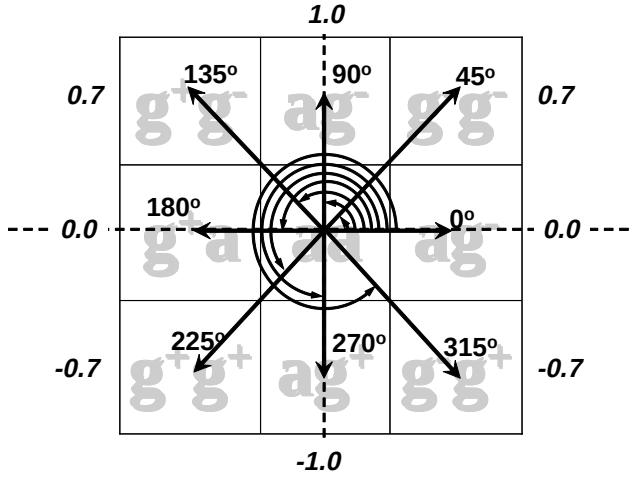

Fig. 9. Definition of conformational position vector as a structural descriptor to be used for structure-stability relationships. The sin of the degree values (inside the box) are shown numerically outside of the box.

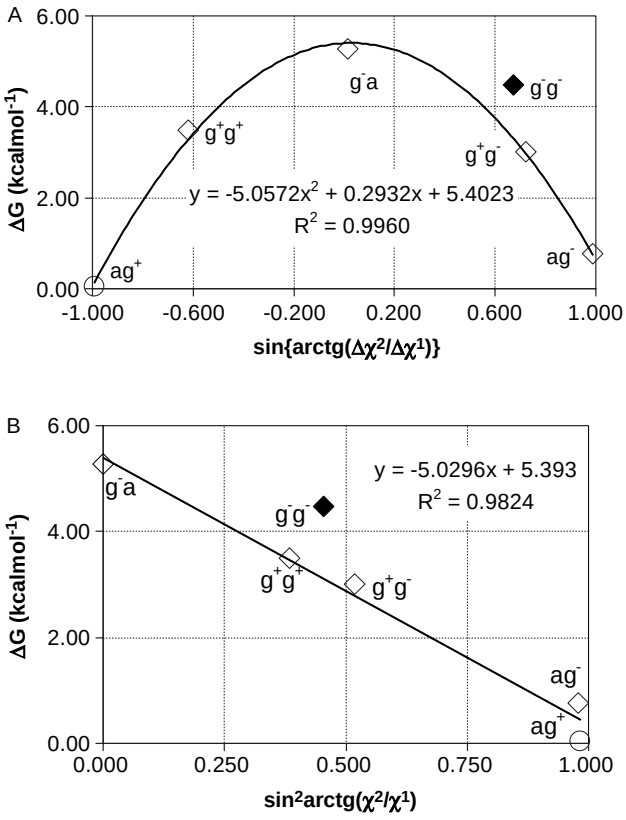

Fig. 10. The Gibbs energies of the six existing minima of MeCO-β_L-Sec-NH-Me against trigonometric functions of the quotient of the two relative dihedral angles of the sidechain ($\Delta\chi^1/\Delta\chi^2$). These points may not be stabilized by SC-BB hydrogen binding while the others might be stabilized more or less to the same degree

Plotting the relative Gibbs free energies of the six existing stable conformers against sin τ yields a concave parabola (Fig. 10(A)). Since ΔG varied quadratically with sin τ plotting those ΔG values against $\sin^2\tau$ leads to an inverse linear relationship (Fig. 10(B)). Analogous relationships but an opposite directional orientation may be obtained by correlating ΔG with cos τ and $\cos^2\tau$.

Table 4
Differencial types of the stabilization of the MeCO-β_L-Sec-NH-Me

Types of stabilisation	Type number	Examples
Hydrogen bonds	1	N(7)–H(12)→:O(10)=C(9)
(a) Backbone→	2	C(19)–H(20,23)→:O(10)=C(9)
backbone	3	C(8)–H(11)→:O(4)=C(3)
(b) Backbone→	4	C(13)–H(16)→:O(10)=C(9)
sidechain		
(i) Se:→H	5	C(13)–H(15–16)→:O(4)=C(3)
(ii) X:→(Se)–H	6	Se(14)–H(17)→:N(7)
(X=O, N)	7	Se(14)–H(17)→:N(18)
	8	Se(14)–H(17)→:O(10)=C(9)
	9	Se(14)–H(17)→:O(4)=C(3)
(c) Sidechain→	10	Se(14):→H(21)–N(18)
backbone	11	Se(14):→H(11)–C(8)
Charge transfer	12	C(3)=O(4):→Se(14)

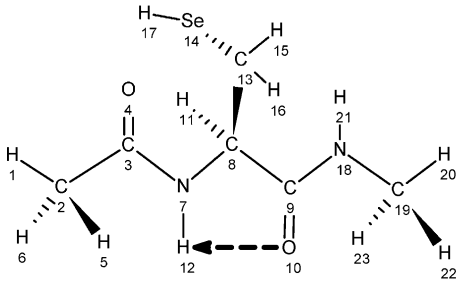

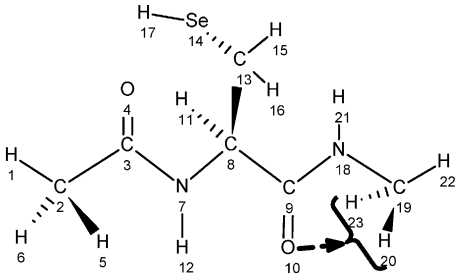

intramolecular hydrogen bond (BB → BB)
Type 2.
distance O·····H (≥ 2.380 Å)
angle: C – H ····· O

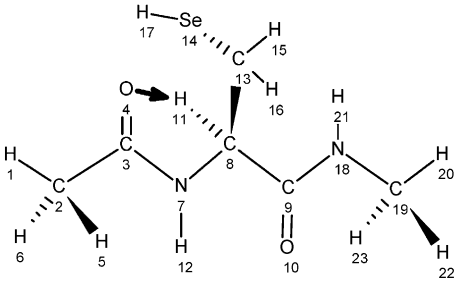

intramolecular hydrogen bond (BB → BB)
Type 3.
distance O·····H (≥ 2.358 Å)
angle: C – O ····· H

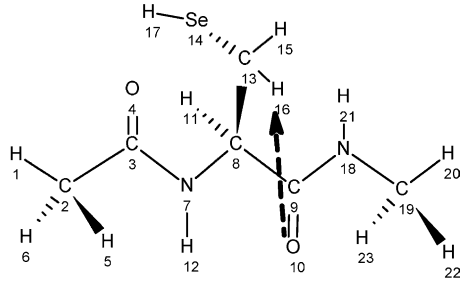

intramolecular hydrogen bond (BB → SC)
Type 4.
distance O·····H (≥ 2.870 Å)
angle: Se – H ····· O

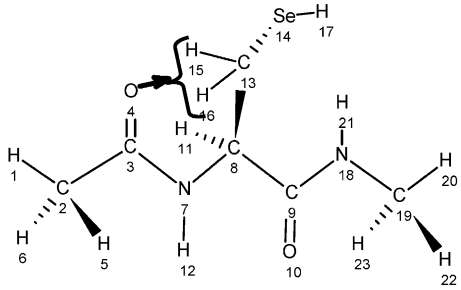

intramolecular hydrogen bond (BB → SC)
Type 5.
distance O·····H (≥ 2.534 Å)
angle: C – O ····· H

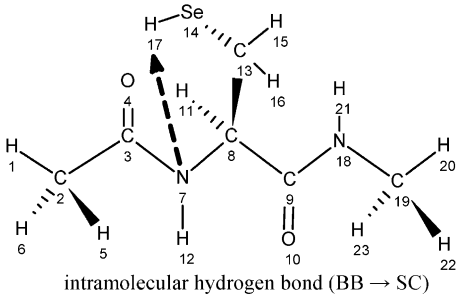

intramolecular hydrogen bond (BB → SC)
Type 6.
distance N·····H (≥ 2.870 Å)
angle: N – H ····· Se

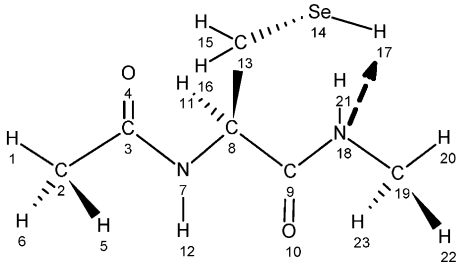

intramolecular hydrogen bond (BB → SC)
Type 7.
distance N·····H (≥ 3.220 Å)
angle: Se – H ····· N

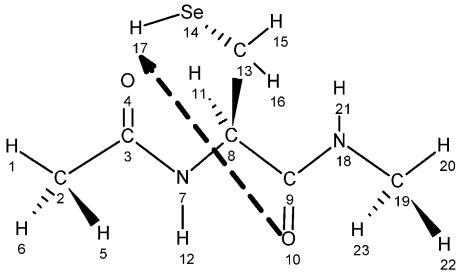

intramolecular hydrogen bond (BB → SC)
Type 8.
distance O·····H (≥ 3.590 Å)
angle: Se – H ····· O

Fig. 11. Various types of intramolecular interaction in MeCO-β_L-Sec-NH-Me (i.e. backbone→sidechain and sidechain→backbone). Limited distances were calculated as the sum of van der Waals radii.

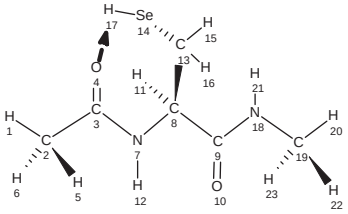

intramolecular hydrogen bond (BB → SC)
Type 9.
distance O·····H (≥ 3.080 Å)
angle: Se – H ····· O

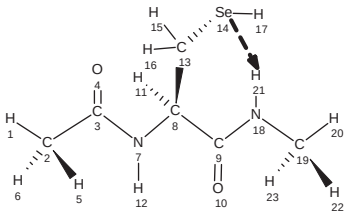

intramolecular hydrogen bond (SC → BB)
Type 10.
distance Se·····H (≥ 2.525 Å)
angle: N – H ····· Se

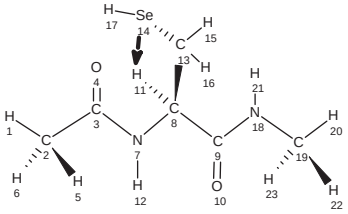

intramolecular hydrogen bond (SC → BB)
Type 11.
distance O·····H (≥ 2.980 Å)
angle: C – H ····· Se

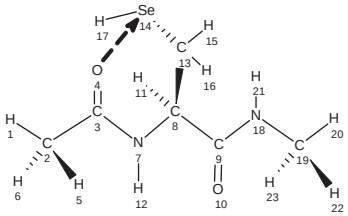

intramolecular charge transfer (BB → SC)
Type 12.
distance O·····H (≥ 3.138 Å)
angle: Se – H ····· O

Fig. 11 (*continued*)

Table 5
Summary of the intramolecular interactions in MeCO-β_L-Sec-NH-Me

Final geometry	ΔE_{rel} (kcal mol^{-1})	Interaction		$\tau_{X\cdots H}$ (Å)	$\alpha_{X\cdots H-Y}$
		Atoms	Type		
ag^-	0.92	O(10)···H(12)N(7)	1	2.10	109.54
		O(4)···H(11)C(8)	3	2.59	88.22
		O(4)···H(15–16)C(13)	5	2.53	116.33
		Se(14)H(17)···N(18)	7	3.22	81.33
		Se(14)···H(21)N(18)	10	2.58	131.29
		Se(14)···H(11)C(8)	11	3.02	76.82
ag^+	0.00	O(10)···H(12)N(7)	1	2.07	110.43
		O(4)···H(11)C(8)	3	2.59	87.86
		O(4)···H(15–16)C(13)	5	2.53	114.69
		Se(14)H(17)···N(18)	7	3.90	57.28
		Se(14)H(17)···O(4)	9	3.91	103.74
		Se(14)···H(21)N(18)	10	2.52	137.53
		Se(14)···H(11)C(8)	11	3.01	77.77
g^-g^-	4.87	O(10)···H(12)N(7)	1	2.38	100.38
		O(10)···H(22)C(19)	2	2.41	101.57
		O(4)···H(11)C(8)	3	2.36	102.12
		O(10)···H(15)C(13)	4	2.87	93.47
		Se(14)H(17)···N(7)	6	3.60	64.27
		Se(14)H(17)···O(4)	9	3.07	96.28
		C(3)O(4)→Se(14)	12	3.55	78.73
g^-a	5.39	O(10)···H(12)N(7)	1	2.36	106.18
		O(4)···H(11)C(8)	3	2.42	97.81
		Se(14) ···H(11)C(8)	11	2.98	75.46
		C(3)O(4)→Se(14)	12	3.12	171.70
g^+g^+	3.89	O(10)···H(12)N(7)	1	2.15	107.90
		O(4)···H(11)C(8)	3	2.56	88.31
		O(4)···H(15–16)C(13)	5	2.60	114.60
		Se(14)H(17)···O(10)	8	3.61	86.22
g^+g^-	3.66	O(10)···H(12)N(7)	1	2.08	107.90
		O(4)···H(11)C(8)	3	2.60	88.31
		O(4)···H(15–16)C(13)	5	2.58	114.59
		Se(14)H(17)···N(7)	6	2.87	49.05
		Se(14)H(17)···O(10)	8	3.91	86.22

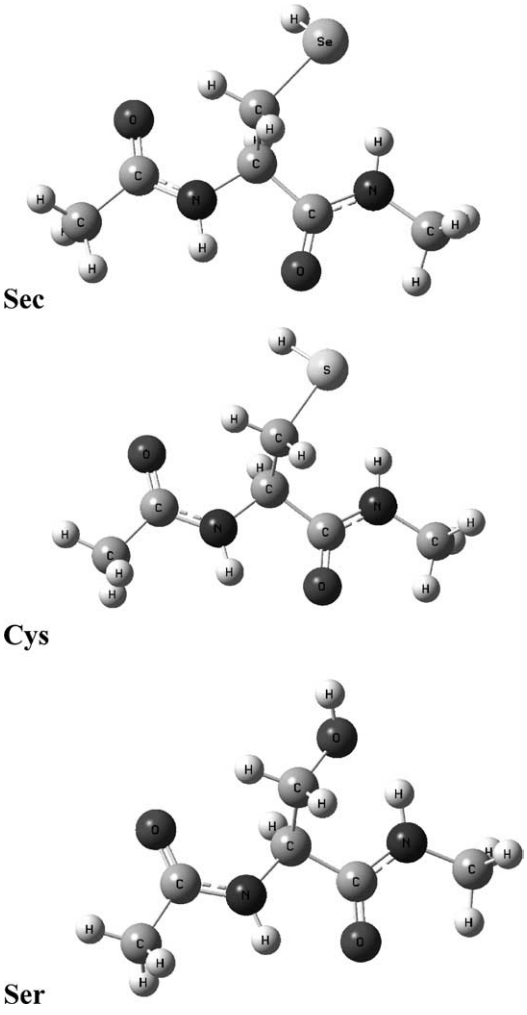

Fig. 12. A comparison of the β_L [ag^+] conformation optimized at the RHF/3-21G level of theory for MeCO-Cys-NH-Me and MeCO-Sec-NH-Me.

The (g^-g^-) conformation on both plots does not correlate well. It seems that this conformer may not be stabilized by SC–BB hydrogen bonding to the same extent as the others; the others might be stabilized more or less to the same degree. The relatively low stability of this conformer may be due to the charge transfer interaction between the Se atom in the sidechain and O(4) in the backbone (see also Table 4 and Fig. 11 type-12 interaction) which may be weaker than an additional hydrogen bond.

3.3. Intramolecular interactions

Two general types of stabilization may be distinguished:

(1) Hydrogen bonding:

$$\begin{array}{ll} \text{C–H}\cdots\text{O}=\text{C} & \text{C–H}\cdots\text{Se} \\ \text{N–H}\cdots\text{O}=\text{C} & \text{N–H}\cdots\text{Se} \\ \text{Se–H}\cdots\text{O}=\text{C} & \text{Se–H}\cdots\text{N} \end{array} \qquad (6)$$

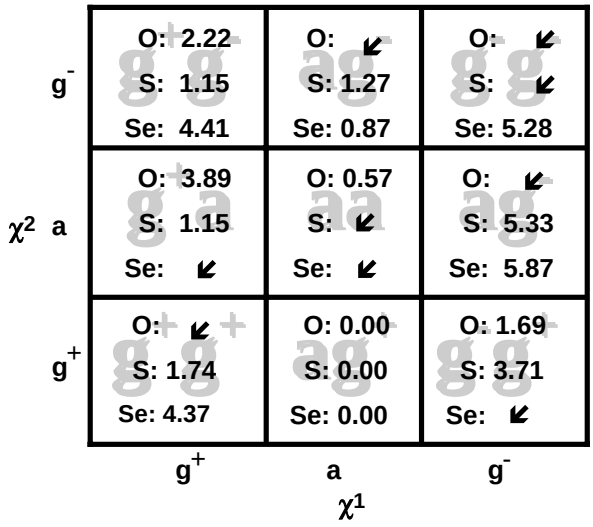

Fig. 13. A schematic representation of the existing minima in β_L-conformations $E=E(\psi,\varphi)$. The global minima in all types of molecules have 0.00 relative energy. Energy values for Ser (O) and Cys (S) were taken from Refs. [37,38] and [39], respectively. The data is also summarized in Table 6.

Hydrogen bonds may exist as:

(a) *backbone→backbone* We have found two types of backbone→backbone interactions: hydrogen bonds exist between H(12) and O(10) atoms as well as between H(20, 23) and O(10) atoms and between H(11) and O(4) atoms, corresponding to Type 1, Type 2 and Type 3, respectively, as shown in Fig. 11 and Table 4.

(b) *backbone→sidechain* In the backbone→sidechain interaction, there are hydrogen bonds between (i) H(15) or H(16) atom associated with O(10) (Type 4) or O(4) (Type 5) as shown in Fig. 11 and Table 4, (ii) H(17) atom which is in the end of the sidechain associated with N(7) (Type 6), N(18) (Type 7), O(10) (Type 8) and O(4) (Type 9) as shown in Fig. 11 and Table 4.

Table 6
A comparison of sidechain dihedral angles of *N*- and *C*-protected Ser [37,38], Cys [39] and Sec computed at the RHF/6-311++G** (Ser), RHF/6-31G(d) (Cys) and B3LYP/6-31G(d) (Sec) levels of theory

χ^1	χ^2	χ^1			χ^2		
		O	S	Se	O	S	Se
g^+	g^-	67.37	65.62	68.06	−66.15	−66.00	−63.75
a	g^-	–	−173.69	−168.00	–	−82.24	−100.57
g^-	g^-	–	−56.68	−51.28	–	−54.41	−62.71
g^+	*a*	70.06	62.84	–	−162.77	−172.79	–
a	*a*	−170.40	–	–	162.56	–	–
g^-	*a*	–	–	−67.37	–	–	−178.60
g^+	g^+	–	55.55	60.18	–	64.26	85.62
a	g^+	−165.68	−160.81	−164.42	89.48	76.44	63.27
g^-	g^+	−94.39	–	–	57.55	–	–

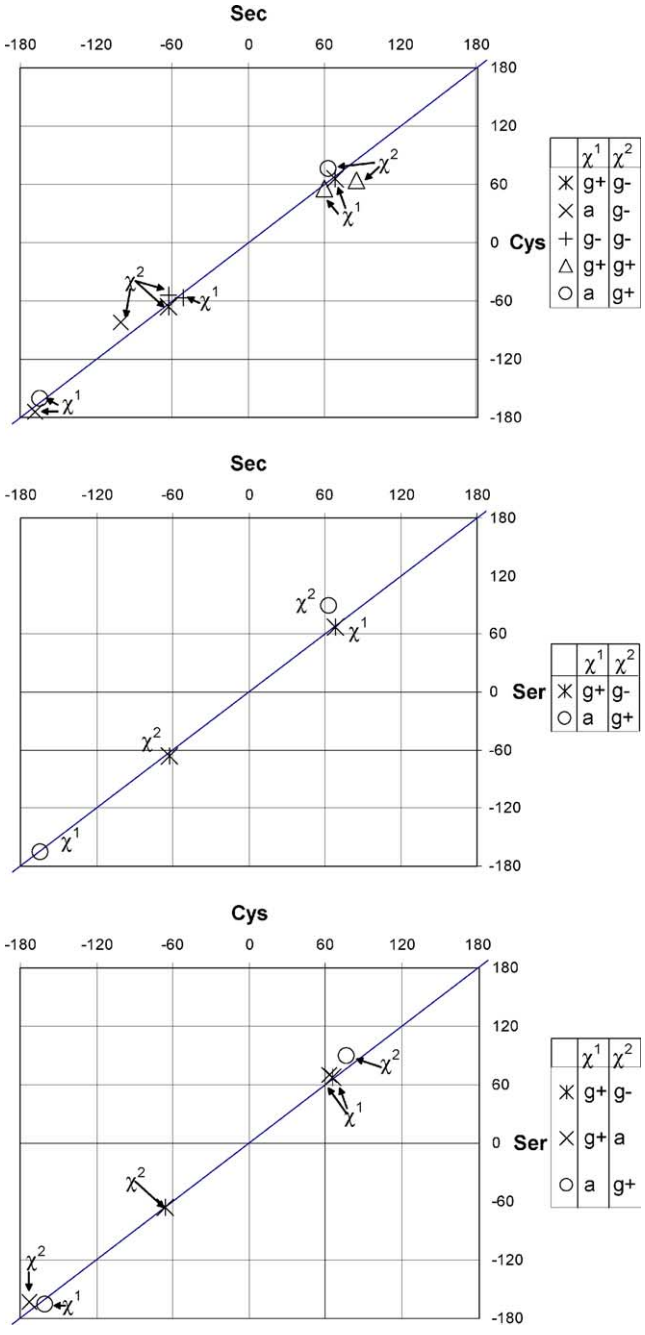

Fig. 14. Correlation of torsion angles for MeCO-β_L-Sec-NH-Me (Sec) and MeCO-β_L-Cys-NH-Me (Cys).

(c) *sidechain → backbone types* The sidechain → backbone interaction is between Se atom and H atom H(21), H(11) (corresponding to Type 10 and 11) as illustrated in Fig. 11 and Table 4.

(2) Charge-transfer interactions:

$$C = O : \rightarrow Se \tag{7}$$

Charge transfer was realized between Se and O atoms (Type 12; see Fig. 11 and Table 4).

In Table 5, the intramolecular interactions are compared for all conformers. This table shows the relative energies of the conformers, the code numbers of interaction types and the location of geometrical characterization of the hydrogen bonds.

The most stable conformer of MeCO-Sec-NH-Me, β_L [ag^+], optimized at the RHF/3-21G level of theory had been compared to that of MeCO-Cys-NH-Me [37,38] and MeCO-Ser-NH-Me [39] in Fig. 12. It can be seen that there is considerable similarity between the corresponding conformers of three amino acid residues.

In Fig. 13 and Table 6, all existing sidechain minima of the β_L backbone structures of MeCO-Ser-NH-Me MeCO-Cys-NH-Me and MeCO-Sec-NH-Me are compared. The global minima for each of three cases is (ag^+). The (g^-g^-) conformer exists only in the case of the Sec residue. Since the atomic radius of Se atom is larger than those of S and O, charge transfer type intramolecular complexation are more likely to occur.

3.4. Comparison of N- and C-protected selenocysteine, cysteine and serine

The two dihedral angles, χ^1 and χ^2, in the sidechain structures (for nomenclature see Fig. 4) in the three congener amino acids are compared. Linear correlations were found for the two dihedral angles associated within all existing conformers of MeCO-Ser-NH-Me, MeCO-Cys-NH-Me and MeCO-Sec-NH-Me. The pair-wise correlations are shown in Fig. 14 for Cys/Sec, Sec/Sec and Sec/Cys. As can be seen, all points associated with the various conformers are fairly close to the 45° lines. This comparison also suggested that the similarity between the O, S and Se

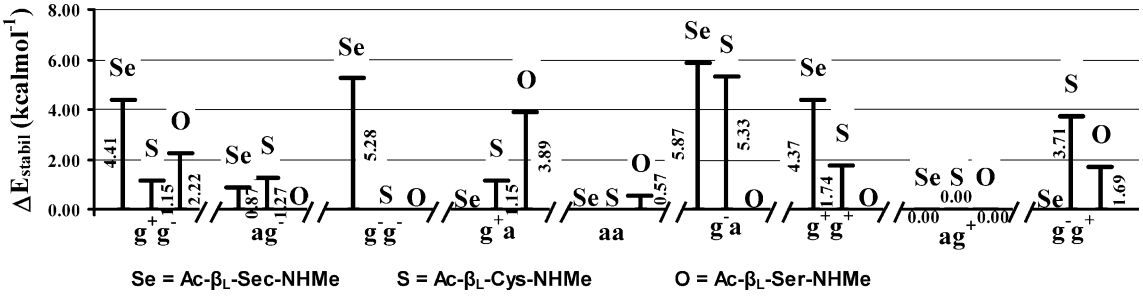

Fig. 15. A graphical comparison for the relative stability energies of the all existing conformation of MeCO-β_L-Sec-NH-Me and MeCO-β_L-Cys-NH-Me.

Table 7
Selected parameters of the Se–Se, Se–S and S–S bridges at the β_L optimized conformer obtained at the RHF/3-21G level of theory

System	Distance (Å)	Total energy (Hartrees)		Redox ΔE^a (kcal/mol)	Dihedral angles											
		Monomer	Dimer		ψ_{i-1}	ω_{i-1}	ϕ_i	ψ_i	ω_{i+1}	φ_{i+1}	χ_i^1	χ_{ij}	χ_i^2	ψ_{j-1}	ω_{j-1}	ϕ_j	ψ_j	ω_{j+1}	ϕ_{j+1}
Se–Se	2.47	−2878.59652	−5756.097458	−17.2	−178.91	−178.01	−163.80	138.40	177.42	−125.84	−166.88	−91.52	−166.88	−178.93	−178.01	−163.81	138.40	177.42	−125.80
Se–S	2.36	–	−3763.162520	−10.2	−178.83	−178.04	−164.51	139.32	177.50	−126.44	−167.41	−94.12	−165.97	−179.44	−178.27	−163.97	138.39	177.17	−124.82
Se–O	1.799	–	−3442.018953	8.3	179.03	−179.39	−163.94	141.34	177.37	−123.79	−165.22	−102.33	−166.92	−177.65	−177.10	−166.11	135.02	178.66	−125.78
S – S	2.25	−885.672747	−1770.224536	−1.3	−179.66	−178.35	−164.61	139.52	177.21	−125.22	−166.45	−96.98	−166.45	−179.52	−178.34	−164.61	139.51	177.22	−125.31
S–O	1.734	–	−1449.076054	20.3	−178.54	−177.90	−165.94	135.72	178.37	−125.80	−165.58	−106.87	−165.42	179.75	−179.94	−164.28	144.29	176.93	−124.56
O–O	1.486	−564.558677	−1127.903616	57.0	177.47	178.73	−165.33	156.66	176.72	−123.51	−159.68	−130.08	−158.01	177.71	179.04	−163.99	153.89	176.77	−124.24

[a] Using $E(H_2) = -1.1229598$ Hartrees.

atoms may lead to analogue structures with similar interactions in spite of the differences in their atomic radii.

An energy comparison is shown in Fig. 15 where the relative energies of the three molecules (MeCO-Ser-NH-Me, MeCO-Cys-NH-Me and MeCO-Sec-NH-Me) were plotted in their respective conformations. The most stable conformation in all of these three cases is (ag^+). It is noteworthy that the (g^-g^-) conformation exists only in the case of Sec. In Sec, charge transfer complexations occur only in g^-a and g^-g^- conformations. These conformations are the least stable as there are only weak intramolecular interactions (see Table 5).

3.5. Comparison of the dimer structures—Se–Se, Se–S and S–S bridges

Table 7 compares the total energies, the relative redox energies and the dihedral angles in the following six possible cases:

$$\begin{array}{lll} \text{O–O} & \text{O–S} & \text{O–Se} \\ & \text{S–S} & \text{S–Se} \\ & & \text{Se–Se} \end{array} \qquad (8)$$

These are fully optimized β_L structures: $\beta_L[a,g^+]\ldots[a,g^+]\beta_L$ constructed from the most stable sidechain conformers corresponding to the $[ag^+]$ sidechain orientation as shown in Fig. 16 for the Se–Se, Se–S and S–S linkages. It may be supposed that the influence of the stability of backbone conformers play only a marginal role to stability of dimers and the nature of the heteroatom is responsible for any trend that may be cure. The energy of the redox reaction, where both X and Y may be O, S and Se,

$$\text{B–X–H} + \text{H–Y–R} \rightarrow \text{R–X–Y–R} + \text{H}_2; \qquad (9)$$

is a function of the X–Y bond length shown in Fig. 17, where the oxygen containing linkages are endothermic. Of the O–O, O–Se and O–Se structures, the O–Se linkage is the least inaccurate. In terms of exothermic characteristics in increasing order of formation, we have shown that the S–S linkage is the least exothermic, followed by the S–Se bond. The Se–Se bond is the most exothermic. Interestingly, the existence of the selenocysteine dimer with the Se–Se linkage has already been reported in the biological literature [40–42]. It may be interesting to note that the nearly thermoneutral S–S linkage is the most frequent and most stable, while the Se–Se linkage occurs the least frequently in biological systems. However, selenodiglutatione (R–Se–Se–R) has been investigated, and has in fact been patented for the inhibition of the proliferation of cancer cells [43]. Some investigations have found that the 'selenotrisulfide' (R–S–Se–S–R) is in fact responsible for the anticarcinogenic activity [44]. The synthesis of tellurocysteine has been achieved [45] but no biological role of Te–Te linkage has been reported.

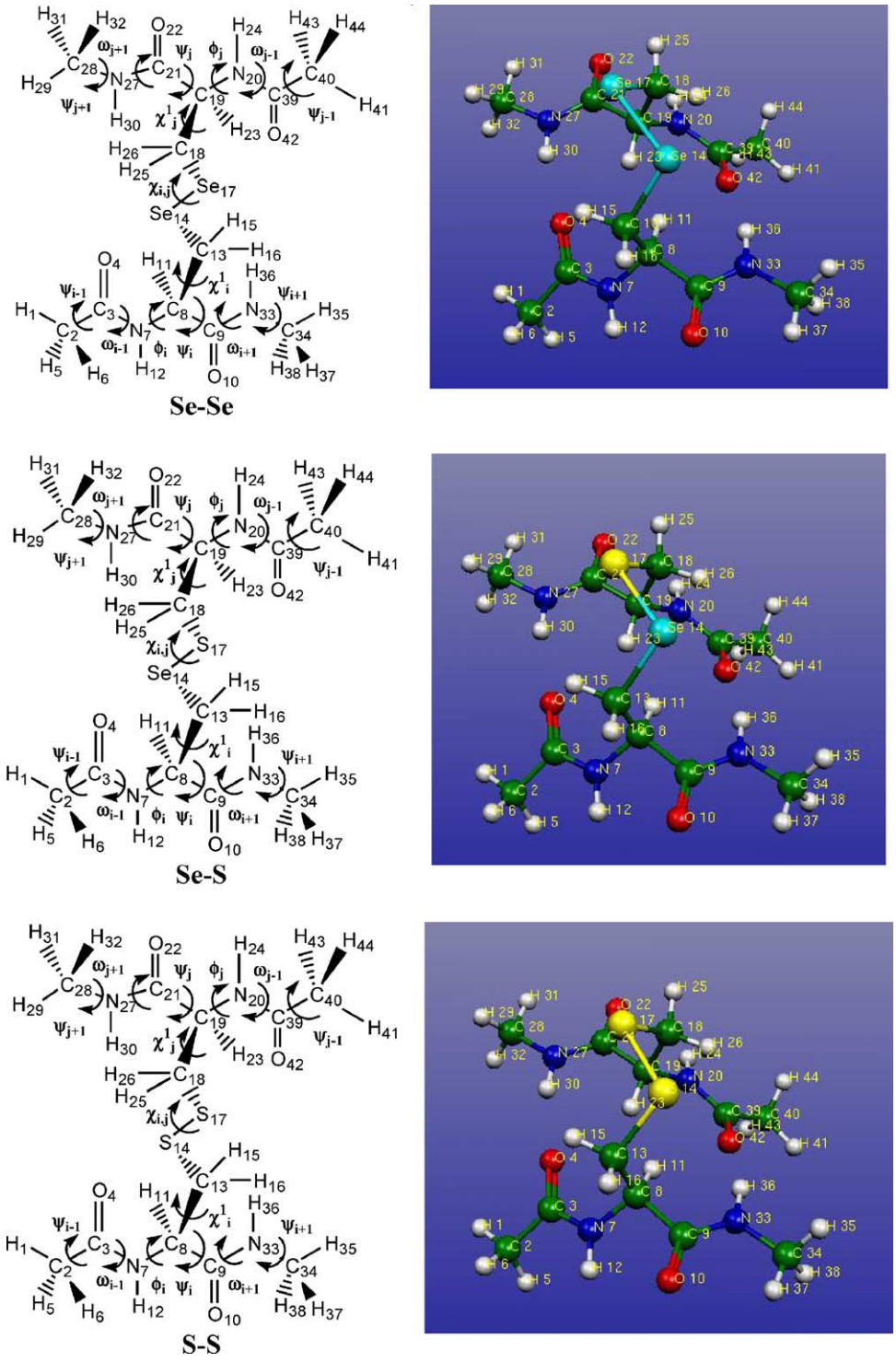

Fig. 16. A schematic illustration of the numbering system applied to the Se–Se, Se–S and S–S bridges as well as the fully optimized β_L structures; $\beta_L[a,a]\cdots[a,a]\beta_L$.

4. Conclusions

The study of sidechain-backbone interactions is very important as has been demonstrated in the case of proline diamide [46]. Undoubtedly these interactions should be studied in all amino acid residues to understand the conformational intricacies involved in peptide folding. Hence from the sidechain conformational analysis of MeCO-Sec-NH-Me in its β_L backbone conformation the following conclusions can be drawn.

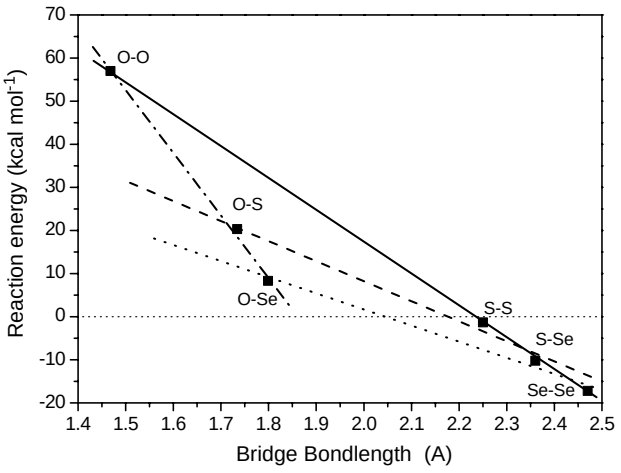

Fig. 17. Dimerization energy of the function of bond length.

Realistically, Sec is expected to have $9^2=81$ conformations [in the backbone: $\psi(g^+,a,g^-)\times\phi(g^+,a,g^-)$; $3^2=9$ and in the sidechain: $\chi^1(g^+,a,g^-)\times\chi^2(g^+,a,g^-)$; $3^2=9$], and thorough investigation of all the torsional modes of the sidechain (χ^1: rotation about the C^α–C^β and χ^2: rotation about the C^β–Se bonds) in the relaxed β_L backbone [(ψ,φ), (a,a)] conformation should therefore yield nine sidechain conformations. However, the relaxed potential energy surface (PES) obtained at the RHF/3-21G level of theory contained seven out of nine minima of the sidechain.

An exploratory structure–stability correlation was attempted for the six stable sidechain conformers and all minima were re-optimized at the RHF/6-31G(d) and B3LYP/6-31G(d) levels of theory. Nevertheless, only two of the minima (g^+a) and (g^-g^+) located at RHF/3-21G level of theory were not found when optimized at higher levels of theory. The frequency calculations of the minima were then used to calculate thermodynamic functions, which gave good correlation for all conformers except g^-g^-. The relative energies of the –CH_2–SeH sidechain conformations have been compared with the relative energies of the analogous –CH_2–SH and –CH_2–OH sidechain conformers, establishing that the global minimum for each of three cases is (ag^+). Oxidative dimerization energies were also estimated, where it was found that the formation of the S–S linkage is slightly exothermic. The S–Se linkage is more exothermic and the Se–Se linkage is the most exothermic.

Acknowledgements

The work has been performed under the Project HPC-EUROPA (RII3-CT-2003-506079), with the support of the European Community-Research Infrastructure Action under the FP6 'Structuring the European Research Area' Programme. The research was also supported partially by grants from the Hungarian Scientific Research Fund (OTKA-F04681).

The authors gratefully thank Suzanne K. Lau for her kind help while preparing this manuscript.

References

[1] T. Finkel, N.J. Holbrook, Nature 408 (2000) 239.
[2] W.A. Pryor, in: H.R. Warner, R.N. Butler, R.L. Sprott (Eds.), Modern Biological Theories of Ageing, Raven, New York, 1987, p. 89.
[3] M.D. Brand, C. Affourtit, T.C. Esteves, K. Green, A.J. Lambert, S. Miwa, J.L. Pakay, N. Parker, Free Rad. Biol. Med. 37 (2004) 755.
[4] T. Fukao, J. Bailey-Serres, Trends Plant Sci. 9 (2004) 449.
[5] B. Halliwell, J.M.C. Gutteridge,, second ed. Free Radicals in Biology and Medicine, Clarendon Press, Oxford, UK, 1989.
[6] J.M. Mates, C. Perez-Gomez, I.N. De Castro, Clin. Biochem. 32 (1999) 595.
[7] J.K. Willcox, S.L. Ash, G.L. Catignani, Crit. Rev. Food Sci. Nutr. 44 (2004) 275.
[8] M.M. Tarpey, I. Fridovich, Circ. Res. 89 (2001) 224.
[9] T. Ozawa, Physiol. Rev. 77 (1997) 425.
[10] K.B. Beckman, B.N. Ames, Physiol. Rev. 78 (1998) 547.
[11] K. Apel, H. Hirt, Annu. Rev. Plant Biol. 55 (2004) 373.
[12] S.C. Gamble, A. Wiseman, P.S. Goldfarb, J. Chem. Tech. Biotech. 68 (1997) 123.
[13] O. Epp, R. Ladenstein, A. Wendel, Eur. J. Biochem. 133 (1983) 51.
[14] D.M. Townsend, K.D. Tew, H. Tapiero, Biomed. Pharm. 57 (2003) 145.
[15] H. Tapiero, D.M. Townsend, K.D. Tew, Biomed. Pharm. 57 (2003) 134.
[16] J. Chen, M.J. Berry, J. Neurochem. 86 (2003) 1.
[17] J.C. Vank, C.P. Sosa, A. Perczel, Csizmadia, Can. J. Chem. 78 (2000) 406.
[18] J.C. Yeung, G.A. Chasse, E.J. Frondozo, L.L. Torday, J.G. Papp, J. Mol. Struct. (Theochem) 546 (2001) 143.
[19] G.A. Chasse, K.P. Chasse, A. Kucsman, L.L. Torday, J.G. Papp, J. Mol. Struct. (Theochem) 571 (2001) 7.
[20] G.A. Chasse, M.L. Mak, E. Deretey, I. Farkas, L.L. Torday, J.G. Papp, D.S.R. Sarma, A. Agarwal, A. Sujak, S. Agarwal, A.V. Rao, J. Mol. Struct. (Theochem) 571 (2001) 27.
[21] D.H. Setiadi, G.A. Chass, J.C. Koo, B. Penke, I.G. Csizmadia, J. Mol. Struct. (Theochem) 666-667 (2003) 439.
[22] D.H. Setiadi, G.A. Chass, L.L. Torday, A. Varro, J.G. Papp, J. Mol. Struct. (Theochem) 637 (2003) 11.
[23] D.H. Setiadi, G.A. Chass, L.L. Torday, A. Varro, J.G. Papp, J. Mol. Struct. (Theochem) 620 (2003) 93.
[24] D.H. Setiadi, G.A. Chass, L.L. Torday, A. Varro, J.Gy. Papp, I.G. Csizmadia, Eur. Phys. J. D 20 (2002) 609.
[25] D.H. Setiadi, G.A. Chass, L.L. Torday, A. Varro, J.G. Papp, J. Mol. Struct. (Theochem) 594 (2002) 161.
[26] V.V. Kónya, G.M. Peter, B. Viskoltz, I.G. Csizmadia, J. Mol. Struct. (Theochem) 666–667 (2003) 397.
[27] R.J. Juhasz, L.F. Pisterzi, D.M. Gasparro, D.R.P. Almeida, I.G. Csizmadia, J. Mol. Struct. (Theochem) 666-667 (2003) 401.
[28] A. Mantas, E. Deretey, F.H. Ferretti, M.R. Estrada, I.G. Csizmadia, J. Mol. Struct. (Theochem) 504 (2000) 77.
[29] K.S. Lau, A. Mantas, G.A. Chass, F.H. Ferretti, M. Estrada, G. Zamarbide, I.G. Csizmadia, Can. J. Chem. 80 (2002) 845.
[30] J.C. Vank, H. Henry-Riyad, I.G. Csizmadia, J. Mol. Struct. (Theochem) 504 (2000) 267.
[31] G.A. Chass, M.A. Sahai, J.M.S. Law, S. Lovas, Ö. Farkes, A. Perczel, J.-L. Rivail, I.G. Csizmadia, Int. J. Quantum Chem. 90 (2002) 933.
[32] M.A. Sahai, G.A. Chass, S. Lovas, B. Penke, G. Csizmadia, J. Mol. Struct. (Theochem) 666–667 (2003) 169.

[33] IUPAC-IUB Commission on Biochemical Nomenclature; Biochemistry 9 (1970) 3471.
[34] M.J. Frisch, G.W. Trucks, H.B. Schlegel, G.E. Scuseria, M.A. Robb, J.R. Cheeseman, J.A. Montgomery, Jr., T. Vreven, K.N. Kudin, J.C. Burant, J.M. Millam, S.S. Iyengar, J. Tomasi, V. Barone, B. Mennucci, M. Cossi, G. Scalmani, N. Rega, G.A. Petersson, H. Nakatsuji, M. Hada, M. Ehara, K. Toyota, R. Fukuda, J. Hasegawa, M. Ishida, T. Nakajima, Y. Honda, O. Kitao, H. Nakai, M. Klene, X. Li, J.E. Knox, H.P. Hratchian, J.B. Cross, C. Adamo, J. Jaramillo, R. Gomperts, R.E. Stratmann, O. Yazyev, A.J. Austin, R. Cammi, C. Pomelli, J.W. Ochterski, P.Y. Ayala, K. Morokuma, G.A. Voth, P. Salvador, J.J. Dannenberg, V.G. Zakrzewski, S. Dapprich, A.D. Daniels, M.C. Strain, O. Farkas, D.K. Malick, A.D. Rabuck, K. Raghavachari, J.B. Foresman, J.V. Ortiz, Q. Cui, A.G. Baboul, S. Clifford, J. Cioslowski, B.B. Stefanov, G. Liu, A. Liashenko, P. Piskorz, I. Komaromi, R.L. Martin, D.J. Fox, T. Keith, M.A. Al-Laham, C.Y. Peng, A. Nanayakkara, M. Challacombe, P.M.W. Gill, B. Johnson, W. Chen, M.W. Wong, C. Gonzalez, J.A. Pople, GAUSSIAN 03, Revision B.05, Gaussian, Inc., Pittsburgh, PA, 2003.
[35] J.G. Angyan, I.G. Csizmadia, R. Daudel, R.A. Poirier, Chem. Phys. Lett. 131 (1986) 247.
[36] A. Perczel, J.G. Angyan, M. Kajtar, W. Viviani, J.L. Rivial, J.F. Marcoccia, I.G. Csizmadia, J. Am. Chem. Soc. 113 (1991) 6256.
[37] J.A. Bombasaro, M.A. Zamora, H.A. Baldoni, R.D. Enriz, J. Phys. Chem., A 109 (2005) 874.
[38] M.A. Zamora, H.A. Baldoni, J.A. Bombasaro, M.L. Mak, A. Perczel, O. Farkas, R.D. Enriz, J. Mol. Struct. (Theochem) 540 (2001) 271.
[39] I. Jákli, A. Perczel, Ö. Farkas, A.G. Császár, C. Sosa, I.G. Csizmadia, J. Comput. Chem. 21 (2000) 626.
[40] N. Esaki, V. Seraneeprakarn, H. Tanaka, K. Soda, J. Bacteriol. 170 (1988) 751.
[41] M. Björnstedt, M. Hamberg, S. Kumar, J. Xue, A. Holmgren, J. Biol. Chem. 270 (1995) 11761.
[42] L.N. Vernie, M. de Vries, L. Karreman, R.J. Topp, S. Bont, Biochem. Biophys. Acta 739 (1983) 1.
[43] F.A. Kralick, W.B. Parrish, D.N. Willett, Method for the inhibition of the proliferation of cancer cells in a tumor sensitive to treatment with a selenodithiol such as selenodiglutatione, United States Patent No. 5 104 (1992) 852.
[44] H. Wen, B. Shi, L.M. Boylan, L. Chen, J.J. Chen, R. Davis, E. Spallholz, Biol. Trace Elem. Res. 58 (1997) 43.
[45] E.M. Stocking, J.N. Schwarz, H. Senn, M. Salzmann, A. Silks, J. Chem. Soc. Perkin Trans. 1 (1997) 2443.
[46] M.A. Sahai, T.A.K. Kehoe, J.C.P. Koo, D.H. Setiadi, G.A. Chass, B. Viskolcz, B. Penke, E.F. Pai, I.G. Csizmadia, J. Phys. Chem. A 109 (2005) 2660.